Enhanced visible light photocatalysis by BN-TiO2 enabled electrospun nanofibers for pharmaceutical degradation and wastewater treatment

Lu Lin, Wenbin Jiang, Maryline Nasr, Mikhael Bechelany, Philippe Miele, Huiyao Wang, Pei Xu

Enhanced visible light photocatalysis by BN-TiO_2 enabled electrospun nanofibers for pharmaceutical degradation and wastewater treatment

Lu Lin [a#], Wenbin Jiang [a#], Maryline Nasr [b], Mikhael Bechelany [b], Philippe Miele [b], Huiyao Wang [a*], Pei Xu [a*]

[a]Department of Civil Engineering, New Mexico State University, 3035 S Espina Street, Las Cruces, NM 88003, USA

[b]Institut Européen des Membranes, IEM, UMR-5635, Université de Montpellier, ENSCM, CNRS, Place Eugène Bataillon, F-34095 Montpellier Cedex 5, France.

[#] These authors contributed equally.

[*]Corresponding author: Huiyao Wang, Email: huiyao@nmsu.edu

[*]Corresponding author: Pei Xu, Email: pxu@nmsu.edu

Abstract

Boron nitride (BN) nanosheets are promising support materials for catalysts. A series of BN-TiO_2 enabled electrospun nanofibers were synthesized for photocatalytic treatment of ibuprofen and secondary wastewater effluent under visible light. X-ray photoelectron spectroscopy confirmed the existence of B-O-Ti bonds between BN nanosheets and TiO_2 nanofibers, resulting in energy rearrangement, narrowed band gap, and enhanced light utilization efficiency of TiO_2-BN nanocomposites in the visible light spectrum. Transient photocurrent measurement revealed that the BN enhanced the transport of photogenerated holes from the bulk TiO_2 nanofibers to its surface, resulting in more efficient separation and less recombination of the charge carriers. Kinetic study of ibuprofen degradation indicated enhanced photocatalytic performance of TiO_2-BN catalysts with higher BN content in the nanocomposites. The kinetic rate constant of TiO_2-10% BN catalysts was 10 times higher than the pure TiO_2 nanofibers. The degradation of organic contaminants in wastewater followed the same trend as ibuprofen and improved with increasing BN content. The stability of the TiO_2-BN nanocomposites as an effective solar photocatalyst was demonstrated by multiple cycles of wastewater treatment. The results proved the TiO_2-BN is an appealing photocatalyst under visible light.

Keywords: TiO_2-BN nanocomposites; visible light photocatalysis; pharmaceuticals; secondary wastewater; organic contaminants degradation; photocurrent measurement

1. Introduction

Many synthetic and naturally occurring chemicals including pharmaceuticals and persistent organic wastewater contaminants have culminated in environment due to the effluent discharge from wastewater treatment plants [1-3]. Despite the low concentrations of the contaminants of emerging concerns, they may cause numerous negative ecological and human health impacts. New advanced techniques are imperative to treat these contaminants in anticipation of more stringent regulations [4].

Many advanced treatment approaches, such as advanced oxidation processes, are available for removal of these emerging contaminants, among them, heterogeneous photocatalysis is an appealing technique to degrade recalcitrant organic contaminants through the utilization of solar energy [5-14]. Various photocatalysts have been investigated including titanium dioxide (TiO_2), zinc oxide, zinc sulfide, ferric oxide, and cadmium sulfide [7, 15-17]. TiO_2 nanoparticles have become a widely used photocatalyst and a benchmark to evaluate newly developed catalysts [5, 18]. Among the different one-dimensional and two-dimensional TiO_2 nanomaterials studied so far, nanofibers (one-dimensional structures) have emerged in heterogeneous catalysts due to their high aspect ratio, superior electron survivability, and well-defined unidirectional channel for electrical carrier transport [19, 20]. Compared to bulk semiconductor materials, the smaller radial dimension and larger surface to volume ratio of nanofiber facilitate active and rapid diffusion of photogenerated electron–hole charge carriers to the catalyst surface [21, 22]. Furthermore, nanofiber structure is an excellent substrate to combine with co-catalysts, leading to effective transfer of photoexcited electrons and holes from the catalyst to redox reactions [22-24].

General synthesis methods of TiO_2 nanostructures include hydrothermal method, vapor-thermal treatment, the colloidal templating method, and electrospinning [21, 22, 25]. Electrospinning is a promising technique because it allows the fabrication of nanofibers with controllable diameters from a few to several hundred of nanometer in a simple and cost-effective way [26].

One of the limitations of TiO_2 as a photocatalyst is the large number of defects that can accelerate the recombination of photogenerated electrons and holes [18, 27]. Modification of TiO_2 with metal/nonmetal ions or other semiconductors, such as iron [28, 29], gold [30], nitrogen [16], silver [31], Bi_2WO_6 [32], chitosan [15], and graphene/graphene oxide [33, 34], is an efficient method to improve its performance. A number of recent studies focus on the combination of TiO_2 with boron nitride (BN) nanosheet because of its large specific surface area and reactive edge structure [35, 36]. BN nanosheet is usually not considered as photocatalyst due to its wide band gap (5.5 eV). However, the exceptional properties, such as excellent chemical inertness, have made the BN nanosheet a promising substrate for other photocatalysts.[37].

Up to date, limited studies have focused on applying TiO_2-BN for water treatment. It has been reported that the recombination of electrons and holes is slowed down when positive holes from the activated TiO_2 are attracted to the BN, which is negatively charged. Thus the photocatalytic degradation ability of TiO_2-BN for Rhodamine B (RhB) and methylene blue (MB) was increased up to 15 and 8 times under ultraviolet (UV) light irradiation, respectively [38]. Nasr *et al.* also found the combination of BN nanosheets with TiO_2 could significantly improve the separation of photogenerated charge carries that can lead to an improved photocatalytic activity under UV irradiation [25]. A recent study by Liu *et al.* [39] also indicated that TiO_2-BN hybrid nanosheets form highly active B-O-Ti bonding structure, extending absorbed light wavelength from UV to visible range, largely enhancing the photocatalytic performance. Currently, most studies on TiO_2-BN

photocatalysis are limited to prepared dyes (e.g., MB, methyl orange, RhB, and violet) [25, 38-44] and phenol solutions [39]. More researches on environmental contaminants like pharmaceuticals and real wastewater are needed.

Although our previous work has demonstrated the incorporation of BN into TiO_2 enhanced photocatalytic oxidation of ibuprofen under UV irradiation [44], investigation of visible light is also crucial for the wider application of TiO_2-BN as solar photocatalysts, especially for treating real wastewater under the impact of organic and inorganic constituents.

In this study, a series of TiO_2 nanofibers enfolded with BN nanosheets were prepared to investigate the photocatalytic performance during treatment of a pharmaceutical and secondary wastewater effluent under visible light irradiation. Ibuprofen was chosen as a model contaminant to gauge the photocatalytic ability of the TiO_2-BN nanocomposites in visible light range. The potential application of the TiO_2-BN nanocomposites for wastewater treatment was also studied under visible light irradiation and analyzed by a suite of analytical methods. The stability and recyclability of the prepared catalysts for treatment of secondary effluent was evaluated by multiple photocatalytic experiments.

2. Experimental Section

2.1. Materials and characterization

In this study, we prepared the TiO_2-BN photocatalysts using the method described by Nasr *et al.* [25]. Synthesized materials with different percentage of BN (10 wt%, 7 wt%, 5 wt%, 3 wt%, and 0 wt%) to Ti were named as TB4, TB3, TB2, TB1, and TiO_2, respectively. H-7650 transmission

electron microscopy (TEM, Hitachi High-Technologies Corp., Pleasanton, California) was used to analyze the morphology of prepared nanofibers. The band gap of the catalysts was calculated based on UV-Vis absorbance (UV-Vis spectrophotometer DR6000; Hach Company, Colorado). Chemical compositions of the catalysts were characterized using a Nicolet iS10 attenuated total reflection Fourier transform infrared spectroscopy (ATR-FTIR, Thermo Fisher Scientific Inc., Massachusetts, USA) and a Kratos Axis 165 Ultra X-ray Photoelectron Spectrometer (XPS, Kratos Analytical Ltd, UK) with a photon energy of 1486.6 eV operated at 15 keV and 20 mA emission current. The photocurrents of the photocatalysts were measured using an electrochemical work station (CHI 760C; CH Instruments Inc., Texas) in a standard three electrodes system with 0.1 M NaCl solution as support electrolyte. The as-prepared nanofibers (TiO_2 and TB4) were dispersed in deionized water and then deposited on a 1 × 1 cm indium tin oxide (ITO) coated glass to be the working electrode. Counter electrode was a Pt wire and reference electrode was an Ag/AgCl electrode.

2.2. Adsorption and photodegradation experiments

The ibuprofen solution of 5 mg/L (Acros Organics Co, New Jersey) was aerated for 8 hours to remove CO_2 and increase dissolve oxygen of the solution (neutral pH). The wastewater was the secondary effluent collected from a wastewater treatment plant in Las Cruces, New Mexico, USA. The treatment process includes roughing filter, primary sedimentation, activated sludge, and secondary sedimentation.

10 mg catalyst sample and 50 mL tested solution were mixed in a 100 mL beaker under visible light to conduct photocatalysis experiments. The visible light was provided by a 150 Watts halogen lamp (JLD-150P, Nanjing Chunhui S&T Industrial Co., China). Photolysis experiment was

conducted in the same condition without catalyst. The solution mixture was magnetically stirred for 2 hours, and samples were taken at 0 min, 10 min, 20 min, 30 min, 60 min, 90 min, and 120 min. Nanofibers were recovered by filtering the final solution through a 0.45 μm cellulose acetate membrane (Toyo Roshi Kaisha, Japan).

Repeated wastewater photocatalytic degradation cycles were performed to gauge the stability and reusability of the photocatalysts under 2-hour visible light irradiation. The spent nanofibers were separated from the suspensions via filtration, and then put into the solution to repeat photocatalytic experiment. After a number of cycles, the used nanofibers were dispersed into 50 mL deionized water under 6 hours of visible light irradiation to regenerate the used nanocomposites.

2.3. Analytical methods

The concentration of ibuprofen was quantified by high performance liquid chromatography (HPLC; PerkinElmer Series 200, Connecticut, USA) with a Discovery C18 column (Sigma Aldrich, Missouri, USA). The mobile phase consisted of 30% 25 mM KH_2PO_4 buffer solution (pH 2.5) and 70% acetonitrile at a flow rate of 1 mL/min.

DOC, SUVA, and fluorescence excitation emission matrices (FEEM) were used to calculate organic removal for the tested solutions. DOC was measured using a Shimadzu TOC-L carbon analyzer (Kyoto, Japan). Fluorescence spectroscopy (Aqualog-UV-800-C; Horiba Instruments Inc., New Jersey) provides a quick and effective characterization and quantification of dissolved organic matter (DOM) with different chemical structure and functional groups. The total/specific peak volume of FEEM was calculated by integration of total/specific FEEM peaks, and the FEEM reduction of specific organic fraction was estimated by the following equation:

$$Reduction = (1-\frac{\text{final specific FEEM peak volume}}{\text{initial specific FEEM peak volume}})\times 100\% \quad (1)$$

Our previous work [34] proposed that the photocatalytic degradation of ibuprofen follows the simplified Langmuir-Hinshelwood kinetics model as the initial concentration at millimolar level (Eq. (2)) [45, 46]:

$$ln\left(\frac{C_0}{C_t}\right) = k_{app}t \quad (2)$$

where C_0 and C_t are the concentrations of ibuprofen (mg/L) at the time 0 and t (min); k_{app} is the apparent first-order rate constant (min^{-1}), which can be influenced by ibuprofen concentration.

3. Results and discussion

3.1. Characterization of the synthesized photocatalysts

Figure 1 shows the ATR-FTIR spectra for TiO_2 and TB4. For both TiO_2 and TB4 nanofibers, the high characteristic absorption band at 600–900 cm^{-1} is caused by the Ti–O bond. While for the composite TB4 nanofibers, an obvious absorption peak of hexagonal B-N band is observed around 1400 cm^{-1} [25], which is also observed in the spectra of BN. Two small peaks of C-H (2900 cm^{-1}) and CO_2 (2350 cm^{-1}) probably came from the precursor of TiO_2 (titanium tetraisopropoxide, polyvinylpyrrolidone, and ethanol) during materials preparation. The TEM micrographs of the synthesized materials demonstrated clear nanofibrous morphology and BN sheet coated nanofibers (Figure 2). Besides, our previous X-ray diffraction (XRD) results suggested the combination of BN nanosheets had negligible impact on TiO_2 crystallization [44].

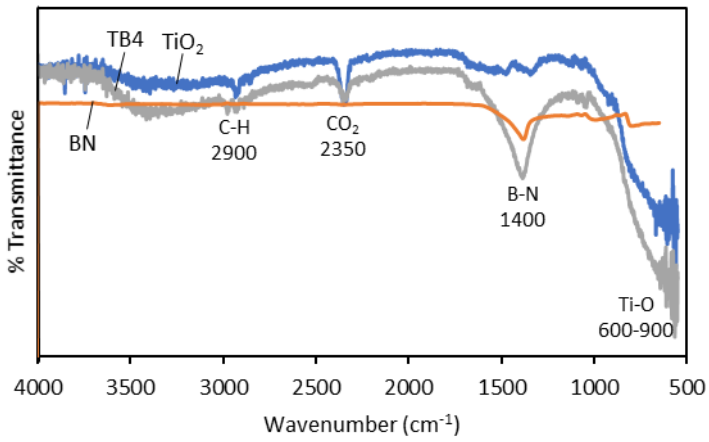

Figure 1. ATR-FTIR spectra of BN, TiO_2 and TB4. BN: boron nitride; TB4: TiO_2-10wt% BN.

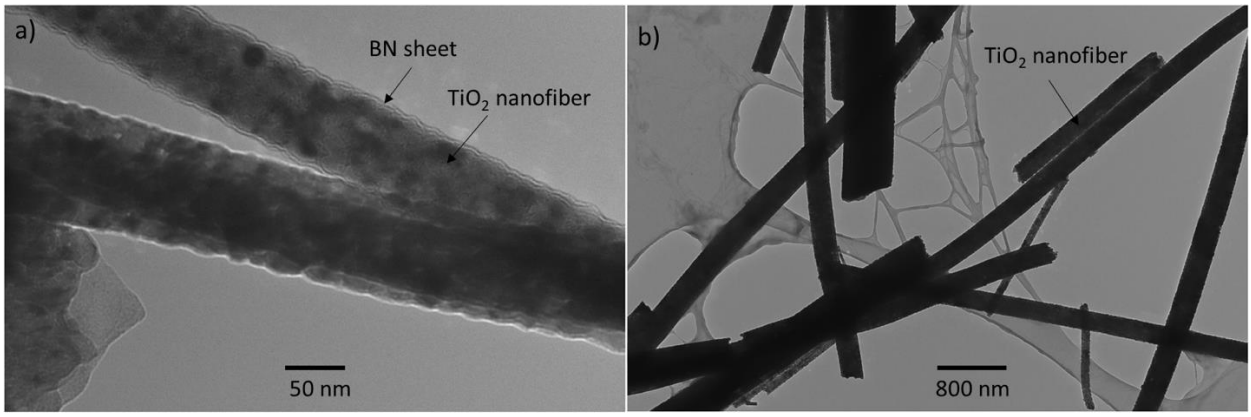

Figure 2. TEM images of (a) TB4 (TiO_2-10wt% BN) and (b) TiO_2.

The interaction between BN nanosheets and TiO_2 nanofibers was further investigated by the XPS analysis. As shown in Figure 3a, two peaks at the binding energy of 190.6 and 191.6 eV in B1s spectra are assigned to the edge or interfacial boron dangling bonds connected with -N and -OH groups, respectively [39, 47]. The peak position of binding energy in B1s spectra shifts for TiO_2 in TB4 samples, at the bind energy of 192.2 eV [39], implying the presence of B-O-Ti bonds in TB4 samples. The existence of B-O-Ti bonds can also be verified by O1s spectra (Figure 3b). The peak at binding energy of 532.0 eV is attributed to the B-O-H bonds referring to surface hydroxyl groups

on BN sheets. The O1s spectra of TB4 consist of two species: Ti-O-Ti (530.1 eV) and B-O-Ti (532.3 eV) bonds [39, 48]. The existence of B-O-Ti bonds in TiO_2-BN samples suggests energy rearrangement, strongly associated with band gap of TiO_2-BN composites. Besides, two characteristic peaks of TiO_2 at 458.9 eV and 464.7 eV are related to $Ti2p_{3/2}$ and $Ti2p_{1/2}$ (Figure 3c).

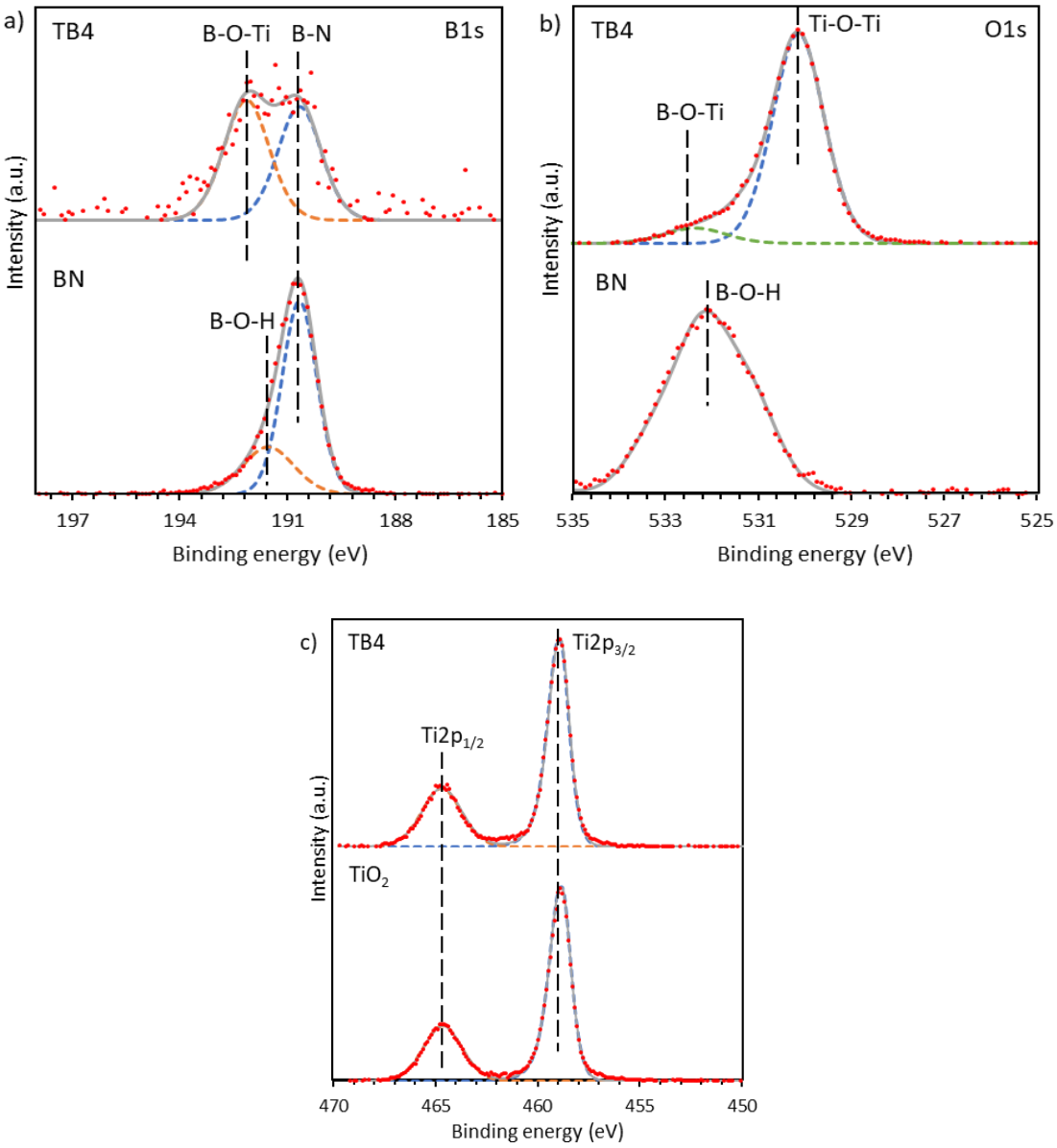

Figure 3. XPS spectra of (a) B1s, (b) O1s, and (c) Ti2p regions for BN, TiO_2 , and TB4. BN: boron nitride; TB4: TiO_2-10wt% BN.

UV-Vis absorption spectra of TiO_2 and TiO_2-BN nanofibers were measured to explore the possible changes in the band gap. Figure 4 shows the Tauc plot of the modified Kubelka-Munk function with a linear extrapolation for each synthesized nanocomposite. The band gaps of the synthesized TiO_2-BN are estimated to be 2.75 eV, narrower than the pure TiO_2 nanofibers (estimated to be 3.20 eV). Hence, the improvement of light utilization was achieved with the incorporation of BN when exposed to visible light; this hypothesis was proven by the photocatalytic degradation of ibuprofen and organics in wastewater. The reduction of band gap may contribute to two aspects. The formation of B-O-Ti bonds (confirmed by XPS analysis) resulted in energy rearrangement, leading to reduced band gap of TiO_2-BN and thereby expanding the absorbed wavelength from UV to visible light spectrum. Meanwhile, Qi *et al.* demonstrated that the band gap of BN nanoribbons can be significantly altered under uniaxial tensile strain, reducing large band gap of BN [49]. It has also been reported that the band gap reduction of monolayer silicane was attributed to the tensile stress of monolayer silicane in the SiH/TiO_2 heterojunction [50]. When the BN nanosheets wrapped on the TiO_2 nanofibers by the electrospinning process, the tensile strain of nanosheets increased. Hence, we could hypothesize that the narrower band gap with increasing BN content may be ascribed to tensile stress of BN nanosheets in TiO_2-BN, resulting in decreased band gap of the TiO_2-BN nanocomposites.

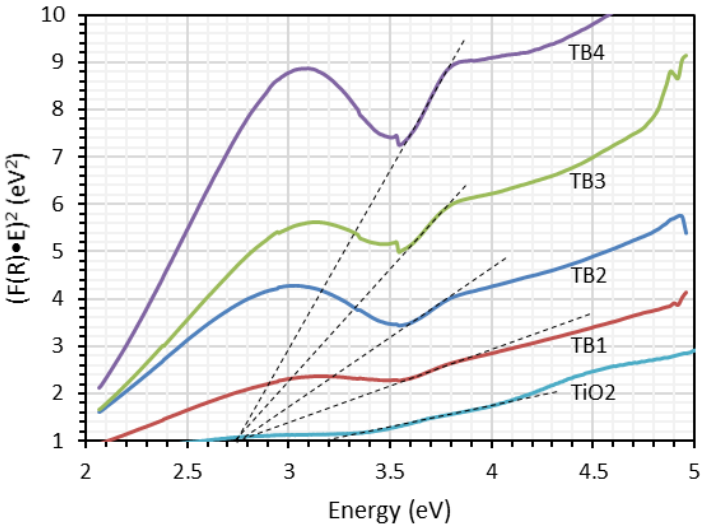

Figure 4. Plot of transformed Kubelka-Munk function $(F(R)\cdot E)^2$ *versus* energy for TiO_2 and TiO_2-BN nanocomposites. TB1: TiO_2-1wt% BN; TB2: TiO_2-3wt% BN; TB3: TiO_2-5wt% BN; TB4: TiO_2-10wt% BN.

The photocurrent spectroscopy is often used to measure transient photocurrent response and study electron-hole transfer mechanism [51]. Figure 5 shows the photocurrent spectroscopy for both TiO_2 and TB4 under visible light irradiation. The TB4 presents a higher photocurrent as compared to the pure TiO_2, suggesting that the transport of charge carriers from the bulk TiO_2 to its surface could be promoted by incorporating BN nanosheets. Most of the studied semiconductors attract photoinduced electrons from TiO_2 as a result of their more positive conduction band level, such as graphene [33], ZnO [52], CdS [53] and SnO_2 [54]. Because surface holes have a much shorter recombination time (about 10 ns) than that of electrons (about 100 ns) [55], the number of interfacial holes often controls the photocatalytic oxidation efficiency [38]. Therefore, improving the transfer of holes may be more vital for the photocatalytic enhancement. Because BN nanosheet has a more negative valence band level than that of TiO_2 (due to a larger band gap compared to the TiO_2), photoinduced holes inject from the TiO_2 nanofibers to the BN nanosheets when they are in contact [38]. Then these

holes migrate to the ITO substrate to produce the final photocurrent, further migration pathway results in improved separation and reduced recombination of the charge carriers in TiO_2-BN nanocomposites. The result of photocurrent measurement confirmed the previous band gap calculations.

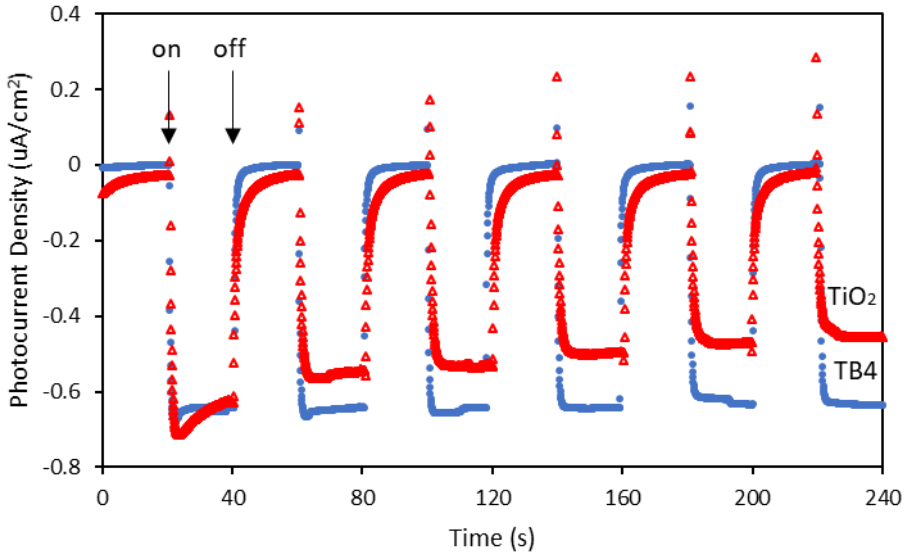

Figure 5. Photocurrent spectra of the prepared pure TiO_2 and TB4 (TiO_2-10wt% BN) exposed to visible light. The applied potential is 0 V vs. Ag/AgCl. "on" and "off" mean visible light was turned on and off, respectively.

3.2. Photocatalytic kinetics of ibuprofen onto the catalysts

The adsorption capacity of a photocatalyst is vital to photocatalysis because the reaction mainly happens on its surface [39]. According to our previous study [44], the specific surface areas of the TiO_2, TB1, TB2, TB3, and TB4 were 19.7, 31.8, 34.4, 48.3, and 49.6 m^2/g, respectively, while

the adsorption of ibuprofen roughly decreased with increasing BN content, with 14.13 mg/g for TiO_2, 13.95 mg/g for TB1, 14.10 mg/g for TB2, 13.77 mg/g for TB3, and 10.28 mg/g for TB4. Introduction of BN into TiO_2 nanofiber decreased the adsorption because both BN and ibuprofen are negatively charged at neutral pH [56].

The photodegradation of ibuprofen under visible light is presented in Figure 6. Oxidation of ibuprofen under direct photolysis without catalyst is negligible after 2-hour exposure. It infers that ibuprofen molecules do not absorb visible light. With the presence of catalyst, photocatalytic activity is improved considerably under visible light. The photocatalytic enhancement enlarges with the growing BN content in the synthesized nanofibers. In order to compare the degradation rates among different catalysts, the Langmuir–Hinshelwood kinetic model (Eq. (2)) was used to fit the experimental data and the rate constants. The model has a good fit on the experimental data with high coefficients of determination ($R^2 > 0.8$). The kinetic rate constant k_{app} follows the order of TB4 (0.0927 min^{-1}), TB3 (0.0632 min^{-1}), TB2 (0.0176 min^{-1}), TiO_2 (0.0097 min^{-1}), and TB1 (0.0091 min^{-1}), consistent with the trend observed in Figure 6. The BN content in TB1 (1wt% BN) is too low to improve photocatalytic performance in comparison with TiO_2. Although both TB3 and TB4 achieve 100% ibuprofen removal after 2-h reaction, higher kinetic rate constant of TB4 implies faster reaction rate compared to TB3. The photocatalytic enhancement of TiO_2-BN can be attributed to their physicochemical properties. First, wrapping BN nanosheets onto TiO_2 nanofibers can improve the separation of charge carriers in the photocatalysts. The negatively charged BN nanosheets can increase the dispersion of photoexcited holes from the TiO_2 nanoparticles, while keeping the generated electrons remain in the TiO_2 nanofibers [25, 38]. As a result, the recombination rate of electron-hole pairs would slow down, and accordingly contribute to the improved photocatalytic performance. Thereby more photoexcited electrons are available in the

nanocomposites to participate in the photodegradation process as compared to the pure TiO_2 nanofibers [25, 38]. Additionally, the incremental absorption intensity of light and the narrower band gap give rise to an enhanced light utilization efficiency of TiO_2-BN. Moreover, the enhanced photocatalytic activity can also be attributed to dispersion stability of the TiO_2 nanoparticles on the BN nanosheets .

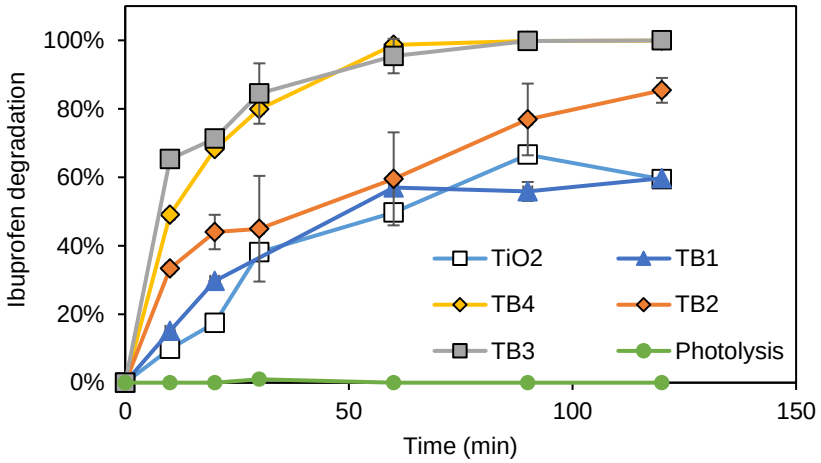

Figure 6. Photocatalytic kinetics of ibuprofen onto the synthesized photocatalysts under visible light. Error bars represent the standard deviation of duplicate experiments. TB1: TiO_2-1wt% BN; TB2: TiO_2-3wt% BN; TB3: TiO_2-5wt% BN; TB4: TiO_2-10wt% BN.

3.3. Photocatalytic treatment of wastewater effluent

Effluents from wastewater treatment plants have been considered an important source of contaminants of emerging concerns in the environment. Because of intricate water chemistry of wastewater effluents, photocatalytic activity could be affected by the presence of substances such as Ca^{2+}, Cl^-, HCO_3^-, SO_4^{2-}, and natural organic matter. Our previous study demonstrated that high ionic strength and divalent ions accelerated photodegradation with Fe-TiO_2, whereas carbonate

species and organic matter inhibited photocatalytic process [29]. The tested wastewater in this study had total dissolved solids (TDS) concentration of 765 mg/L, dissolved organic carbon (DOC) of 16.6 mg/L, alkalinity of 111 mg/L as $CaCO_3$, and pH 7.5. Specific UV absorbance (SUVA) was 7.6 L/mg-m, determined by dividing the UV absorbance at 254 nm by the corresponding DOC concentration.

Moreover, conventional wastewater treatment in wastewater treatment plants relies on primary and secondary treatments to separate suspended solids and eliminate dissolved organic substances. Although ibuprofen has been widely detected in primary wastewater, the removal efficiency after secondary biological treatments is usually over 90% [57-60]. In this study, only weak ibuprofen peaks were detected in the secondary wastewater effluent samples using high resolution mass spectrometry, performed by an Orbitrap Fusion mass spectrometer (ThermoFisher, San Jose, CA) equipping with an Advion NanoMate (Advion, Ithaca, NY). Therefore, we investigated the efficacy of photocatalysis on removal of bulk organic contaminants from secondary wastewater.

The photocatalytic treatment of wastewater was evaluated by DOC, SUVA, and FEEM results (Figure 7). DOC is the organic carbon concentration of all organic compounds in wastewater to assess the mineralization extent of the photocatalysis. The aromatic fractions in the wastewater samples can be evaluated by the SUVA values. The decrease of DOC and SUVA values suggested the removal of organic carbon and aromatic compounds in the treated secondary effluent samples. Interestingly, the decomposition of aromatic organics (in terms of SUVA) enhances remarkably with larger BN content in the catalysts, although the pure TiO_2 and TB1 has 4-11% higher DOC removal than the TB2 and TB3. The TB4 achieves the highest photocatalytic performance for both decomposition (34%) and mineralization (32%). This implies that photocatalytic oxidation is a multi-step process. At low BN content (pure TiO_2 and TB1), catalysts mainly react with small

organic compounds in wastewater then mineralize them into inorganic carbon (HCO_3^-, CO_3^{2-}, and CO_2). With the increase of BN content, the decomposition of large and complex aromatic compounds to intermediates occurs predominately for the TB2 and TB3, resulting in a higher removal of aromatic compounds (SUVA) compared to DOC reduction. The highest photocatalytic activity of the TB4 gives rise to the best performance in both decomposition and mineralization. As discussed in section 3.2, because the ibuprofen kinetic rate measured by HPLC is the decomposition rate from ibuprofen to intermediates, the photocatalysis results from ibuprofen degradation agree with the decomposition trend observed for wastewater from the SUVA and DOC measurements.

The reduction in the FEEM total peak volume (normalized to DOC concentration) has a similar trend as the SUVA values (Figure 7). In Figure 8, four excitation-emission peaks are observed at each zone: 225 nm/360 nm, 225 nm/400 nm, 275 nm/360 nm, and 340 nm/425 nm, corresponding to protein-like, fulvic-like, microbial byproduct-like, and humic-like organic substances, respectively. Secondary wastewater effluent is a mixture of water, organic and inorganic substances from wastewater influent, and biodegradation products from activated sludge system. To evaluate the photocatalytic treatment on characteristic organic matter fractions in wastewater, the fluorescence volume (normalized to DOC concentration) was calculated. As shown in Figure 9, the treatment efficiency of each organic matter fractions improves with increasing BN content in the nanofibers, agreeing with the result of kinetic rate constant calculation in Section 3.2. The synthesized materials have higher treatment efficiency on humic-like substance than others, especially for the pure TiO_2, TB1 and TB2, less than 4% degradation for biological organic matter. With the increasing BN dose, the photocatalytic activity for all organic fractions is

improved significantly; the TB4 achieves 52%, 50%, 46%, and 58% removal for protein-like, fulvic-like, microbial-like, and humic-like substances, respectively.

According to the hydrophilicity, organic matter can be also classified into four characteristic fractions as hydrophobic, slightly hydrophobic substances, hydrophilic charged, hydrophilic neutral substances, ascribed to humic acids, fulvic acids, proteins, and microbial byproducts, respectively [61, 62]. As shown in Figure 9, the removal of humic-like substance is over three times higher than other organic fractions for pure TiO_2, which implies that TiO_2 prefers hydrophobic substances. This may attribute to 53% humic-like substance in wastewater. With the increasing BN content, the removal of protein-, fulvic-, and microbial-like substances increases dramatically and the removal of humic-like substance is doubled. Despite the relatively low content of these organic fractions in wastewater (protein 10%, fulvic 27%, and microbial 9%), their treatment efficiencies are comparable to humic-like substance. It suggested that the incorporation of BN accelerates the degradation of hydrophilic substances, in accord with the hydrophilic property of BN nanosheet [63]. Moreover, the TB4 adsorbs 14%, 4%, 8%, and 17% of protein-, fulvic-, microbial-, and humic-like substances, respectively, after 2-hour dark experiment. The adsorption of hydrophilic substances (e.g., protein and microbial) is close to hydrophobic organics (e.g., humic and fluvic), while the hydrophobic content in wastewater is over four times higher than hydrophilic organics. Thus, the inclined adsorption accelerates the photocatalytic treatment of hydrophilic substances. Because only adsorbed organics can be photocatalytically degraded [29], adsorption of organics might be the control step of wastewater photocatalysis due to low adsorption.

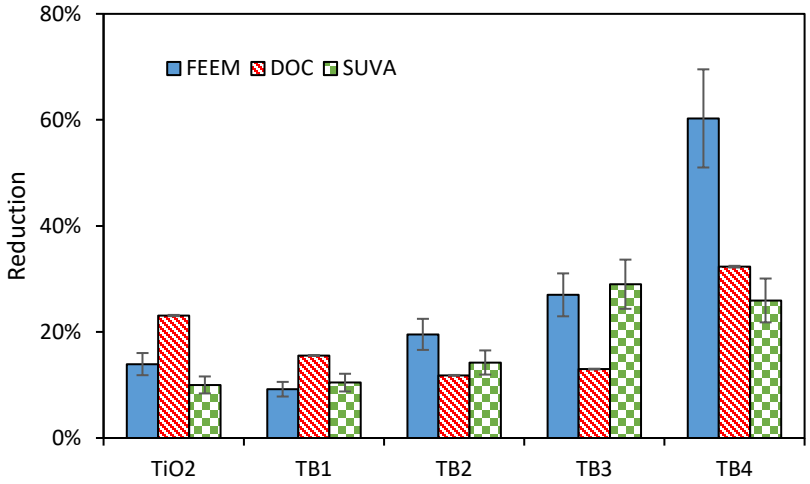

Figure 7. Photocatalytic treatment of wastewater with different catalysts after 2-hour visible light irradiation in terms of reduction in DOC concentration, FEEM total peak volume, and SUVA values. Error bars represent the standard deviation of duplicate experiments. TB1: TiO_2-1wt% BN; TB2: TiO_2-3wt% BN; TB3: TiO_2-5wt% BN; TB4: TiO_2-10wt% BN.

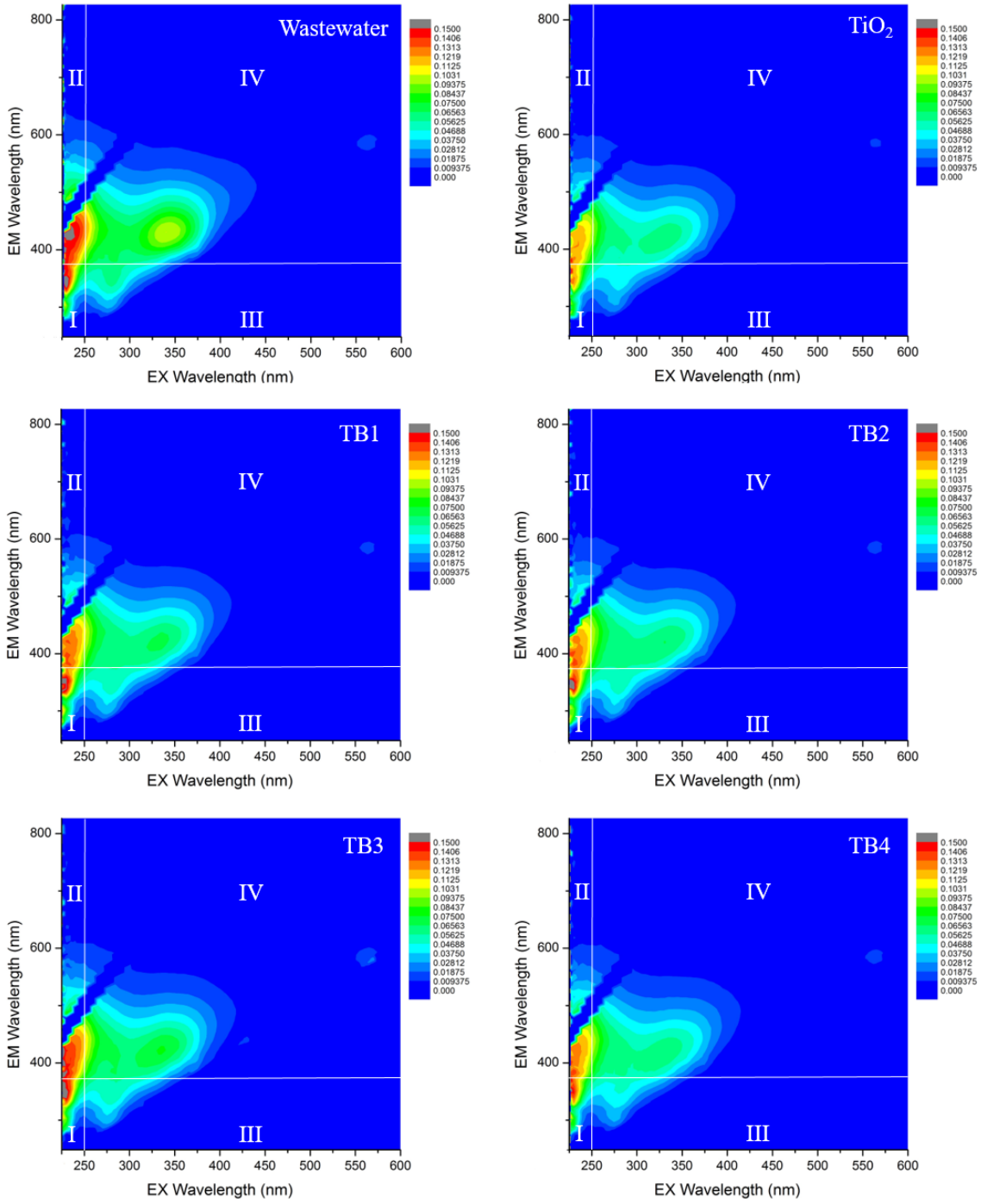

Figure 8. FEEM spectra of wastewater after 2-hour treatment with different photocatalysts. Note: Zones I corresponds to aromatic proteins; Zone II to fulvic acid-like compounds; Zone III to

soluble microbial byproduct-like material; and Zone IV to humic acid-like organics. TB1: TiO_2-1wt% BN; TB2: TiO_2-3wt% BN; TB3: TiO_2-5wt% BN; TB4: TiO_2-10wt% BN.

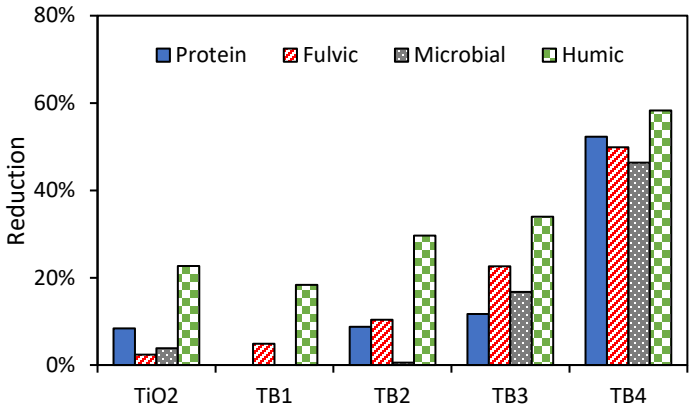

Figure 9. Photocatalytic treatment of wastewater with different catalysts after 2-hour visible light irradiation in terms of different FEEM peak volumes. TB1: TiO_2-1wt% BN; TB2: TiO_2-3wt% BN; TB3: TiO_2-5wt% BN; TB4: TiO_2-10wt% BN.

3.4. Recovery and regeneration of photocatalysts for wastewater effluent treatment

The reusability and regeneration of photocatalysts are important in determining the practical potential of a catalyst. Since the TB4 exhibited the highest photocatalytic activity, the reusability and regeneration of the TB4 were investigated by performing multiple 2-hour photocatalysis cycles treating secondary effluent exposed to visible light. As shown in Figure 10, the decomposition and mineralization efficiencies of wastewater reduce gradually during the five cycles of photocatalytic reaction. The removal efficiencies decrease to 19%, 5%, and 13% for FEEM, DOC, and SUVA, respectively, after five cycles. The reduced photocatalytic performance may attribute to the salts and organics from wastewater or the generated intermediates during

oxidation, these chemicals accumulated in the catalyst may hinder the further wastewater treatment. After 6-hour regeneration by visible light irradiation, the treatment efficiencies are almost recovered compared to the first cycle, which are 57%, 18%, and 12% removal for FEEM, DOC, and SUVA, respectively, suggesting the synthesized catalysts can be easily regenerated.

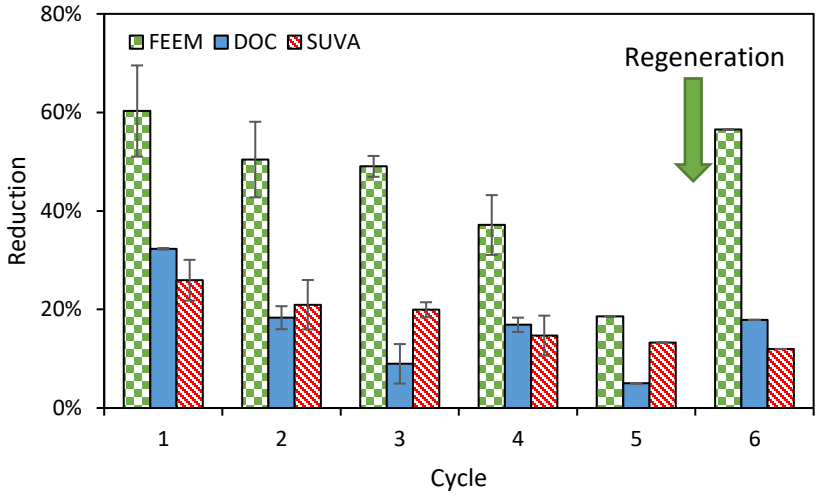

Figure 10. Photocatalytic treatment of wastewater with TB4 (TiO_2-10wt% BN) along repeated and regenerated cycles with visible light in terms of DOC, FEEM total peak volume, and SUVA.

4. Conclusions

Novel TiO_2-BN nanocomposites were synthesized and their environmental application as an appealing photocatalyst for the treatment of ibuprofen and secondary effluent under visible light was investigated. The successful preparation of BN nanosheets wrapped TiO_2 nanofibers was demonstrated by the FTIR spectrum. XPS analysis confirmed the generation of B-O-Ti bonds in the synthesis process, implying the energy rearrangement of TiO_2-BN nanocomposites as a result of reduced band gap. UV-Vis absorption spectra suggested the TiO_2-BN composites had narrower

band gap than the pure TiO_2 nanofiber. A higher photocurrent was measured for the TiO_2-BN nanocomposites compared to the pure TiO_2, implying the transport of holes to TiO_2 surface was promoted through the combination of negative BN nanosheets, resulting in more efficient separation and reduced recombination of charge carriers in TiO_2-BN nanocomposites.

In photocatalytic kinetic study, the TB4 had the highest photocatalytic activity in treating ibuprofen with visible light. The kinetic rate constant of TB4 was almost 10 times larger than pure TiO_2. The successful municipal wastewater secondary effluent treatment with the TB4 further demonstrated its visible-light-driven characteristic. Photocatalytic decomposition and mineralization of wastewater were analyzed in terms of DOC, SUVA, and FEEM reductions. The TB4 achieved the best photocatalytic performance for both decomposition (34%) and mineralization (32%) of wastewater, specifically, the treatment efficiencies reached 52%, 50%, 46%, and 58% for protein-, fulvic-, microbial-, and humic-like substances from wastewater, respectively. Several photocatalytic cycles were repeated to further study the stability of the catalysts, which was successfully regenerated using visible light irradiation. This work provides a fundamental knowledge for further design of advanced hybrid solar photocatalysts and understand the catalysts and water chemistry during degradation of organic contaminants. Photocatalysis can be used as a polish process to further improve effluent water quality prior to reuse.

Conflicts of interest

There are no conflicts to declare.

Acknowledgments

The authors acknowledge the support from the Thomas Jefferson Fund, the Embassy of France in the United States, and the United States National Science Foundation (NSF) Engineering Research Center Program under Cooperative Agreement EEC-1028968 (ReNUWIt).

References

1. E. National Academies of Sciences and Medicine, *The Drug Development Paradigm in Oncology: Proceedings of a Workshop*, National Academies Press, 2018.
2. E. National Academies of Sciences and Medicine, *A Review of the Environmental Protection Agency's Science to Achieve Results Research Program*, The National Academies Press, Washington, DC, 2017.
3. N. R. Council, *Water Reuse: Potential for Expanding the Nation's Water Supply Through Reuse of Municipal Wastewater*, The National Academies Press, Washington, DC, 2012.
4. R. Velagaleti and M. Gill, ACS Publications, 2001.
5. N. F. Moreira, C. Narciso-da-Rocha, M. I. Polo-López, L. M. Pastrana-Martínez, J. L. Faria, C. M. Manaia, P. Fernández-Ibáñez, O. C. Nunes and A. M. Silva, *Water research*, 2018, **135**, 195-206.
6. X. Chen, L. Liu, Y. Y. Peter and S. S. Mao, *Science*, 2011, 1200448.
7. C. R. Stephenson, T. P. Yoon and D. W. MacMillan, *Visible Light Photocatalysis in Organic Chemistry*, John Wiley & Sons, 2018.
8. P. Kar, T. K. Maji, P. K. Sarkar, P. Lemmens and S. K. Pal, *Journal of Materials Chemistry A*, 2018, **6**, 3674-3683.
9. N. Singh, J. Prakash, M. Misra, A. Sharma and R. K. Gupta, *ACS Applied Materials & Interfaces*, 2017, **9**, 28495-28507.
10. M. Misra, N. Singh and R. K. Gupta, *Catalysis Science & Technology*, 2017, **7**, 570-580.
11. N. Singh, J. Prakash and R. K. Gupta, *Molecular Systems Design & Engineering*, 2017, **2**, 422-439.
12. A. Tyagi, K. M. Tripathi, N. Singh, S. Choudhary and R. K. Gupta, *RSC Advances*, 2016, **6**, 72423-72432.
13. N. Singh, K. Mondal, M. Misra, A. Sharma and R. K. Gupta, *RSC Advances*, 2016, **6**, 48109-48119.
14. M. Misra, R. K. Gupta, A. Paul and M. Singla, *Journal of Power Sources*, 2015, **294**, 580-587.
15. R. Saravanan, J. Aviles, F. Gracia, E. Mosquera and V. K. Gupta, *International journal of biological macromolecules*, 2018, **109**, 1239-1245.
16. W. Wang, M. O. Tadé and Z. Shao, *Progress in Materials Science*, 2018, **92**, 33-63.
17. C. Byrne, G. Subramanian and S. C. Pillai, *Journal of Environmental Chemical Engineering*, 2018, **6**, 3531-3555.
18. K. Nakata and A. Fujishima, *Journal of Photochemistry and Photobiology C: Photochemistry Reviews*, 2012, **13**, 169-189.
19. Y. Liu, H. Wang, Y. Wang, H. Xu, M. Li and H. Shen, *Chemical Communications*, 2011, **47**, 3790-3792.
20. J. H. Bang and P. V. Kamat, *Advanced Functional Materials*, 2010, **20**, 1970-1976.
21. R. Al-Attabi, Y. Morsi, J. A. Schütz and L. F. Dumée, *Science of The Total Environment*, 2019, **647**, 725-733.

22. C. Ligon, K. Latimer, Z. D. Hood, S. Pitigala, K. D. Gilroy and K. Senevirathne, *RSC advances*, 2018, **8**, 32865-32876.
23. A. Merenda, L. Kong, N. Fahim, A. Sadek, E. L. H. Mayes, A. Hawley, B. Zhu, S. R. Gray and L. F. Dumée, *ACS Applied Nano Materials*, 2019, **2**, 1951-1963.
24. A. Merenda, A. Rana, A. Guirguis, D. M. Zhu, L. Kong and L. F. Dumée, *The Journal of Physical Chemistry C*, 2019, **123**, 2189-2201.
25. M. Nasr, R. Viter, C. Eid, R. Habchi, P. Miele and M. Bechelany, *New Journal of Chemistry*, 2017, **41**, 81-89.
26. C. Eid, E. Assaf, R. Habchi, P. Miele and M. Bechelany, *RSC Advances*, 2015, **5**, 97849-97854.
27. L. Lin, H. Wang, H. Luo and P. Xu, *Journal of Photochemistry and Photobiology A: Chemistry*, 2015, **307-308**, 88-98.
28. M. Asiltürk, F. Sayılkan and E. Arpaç, *Journal of Photochemistry and Photobiology A: Chemistry*, 2009, **203**, 64-71.
29. L. Lin, H. Wang, H. Luo and P. Xu, *Photochem Photobiol*, 2016, **92**, 379-387.
30. O. A. Krysiak, P. J. Barczuk, K. Bienkowski, T. Wojciechowski and J. Augustynski, *Catalysis Today*, 2019, **321-322**, 52-58.
31. M. Plodinec, I. Grčić, M. G. Willinger, A. Hammud, X. Huang, I. Panžić and A. Gajović, *Journal of Alloys and Compounds*, 2019, **776**, 883-896.
32. S. Murcia-López, M. C. Hidalgo and J. A. Navío, *Applied Catalysis A: General*, 2012, **423-424**, 34-41.
33. L. Lin, H. Wang and P. Xu, *Chemical Engineering Journal*, 2017, **310**, 389-398.
34. L. Lin, H. Wang, W. Jiang, A. R. Mkaouar and P. Xu, *Journal of Hazardous Materials*, 2017, **333**, 162-168.
35. M. Öner, A. Çöl, C. Pochat-Bohatier and M. Bechelany, *RSC Advances*, 2016, **6**, 90973-90981.
36. V. Thangaraj, J. Bussiere, J. M. Janot, M. Bechelany, M. Jaber, S. Subramanian, P. Miele and S. Balme, *European Journal of Inorganic Chemistry*, 2016, **2016**, 2125-2130.
37. J. Biscarat, M. Bechelany, C. Pochat-Bohatier and P. Miele, *Nanoscale*, 2015, **7**, 613-618.
38. X. Fu, Y. Hu, Y. Yang, W. Liu and S. Chen, *Journal of Hazardous Materials*, 2013, **244-245**, 102-110.
39. D. Liu, M. Zhang, W. Xie, L. Sun, Y. Chen and W. Lei, *Applied Catalysis B: Environmental*, 2017, **207**, 72-78.
40. Y. Sheng, J. Yang, F. Wang, L. Liu, H. Liu, C. Yan and Z. Guo, *Applied Surface Science*, 2019, **465**, 154-163.
41. D. Liu, W. Cui, J. Lin, Y. Xue, Y. Huang, J. Li, J. Zhang, Z. Liu and C. Tang, *Catalysis Communications*, 2014, **57**, 9-13.
42. Y. Ide, F. Liu, J. Zhang, N. Kawamoto, K. Komaguchi, Y. Bando and D. Golberg, *Journal of Materials Chemistry A*, 2014, **2**, 4150-4156.
43. M. Nasr, L. Soussan, R. Viter, C. Eid, R. Habchi, P. Miele and M. Bechelany, *New Journal of Chemistry*, 2018, **42**, 1250-1259.
44. L. Lin, W. Jiang, M. Bechelany, M. Nasr, J. Jarvis, T. Schaub, R. R. Sapkota, P. Miele, H. Wang and P. Xu, *Chemosphere*, 2019, **220**, 921-929.
45. A. Houas, H. Lachheb, M. Ksibi, E. Elaloui, C. Guillard and J.-M. Herrmann, *Applied Catalysis B: Environmental*, 2001, **31**, 145-157.
46. I. K. Konstantinou and T. A. Albanis, *Applied Catalysis B: Environmental*, 2004, **49**, 1-14.
47. D. Chen, D. Yang, Q. Wang and Z. Jiang, *Industrial & Engineering Chemistry Research*, 2006, **45**, 4110-4116.
48. W. Zhang, Y. Tang, D. Du, J. Smith, C. Timchalk, D. Liu and Y. Lin, *Talanta*, 2013, **114**, 261-267.
49. J. Qi, X. Qian, L. Qi, J. Feng, D. Shi and J. Li, *Nano Lett*, 2012, **12**, 1224-1228.

50. M. Niu, D. Cheng and D. Cao, *Scientific Reports*, 2014, **4**, 4810.
51. N. Wu, H. Wei and L. Zhang, *Environmental Science & Technology*, 2012, **46**, 419-425.
52. S. Liao, H. Donggen, D. Yu, Y. Su and G. Yuan, *Journal of Photochemistry and photobiology A: Chemistry*, 2004, **168**, 7-13.
53. H. Tada, T. Mitsui, T. Kiyonaga, T. Akita and K. Tanaka, *Nature materials*, 2006, **5**, 782.
54. J. Shang, W. Yao, Y. Zhu and N. Wu, *Applied Catalysis A: General*, 2004, **257**, 25-32.
55. M. R. Hoffmann, S. T. Martin, W. Choi and D. W. Bahnemann, *Chemical reviews*, 1995, **95**, 69-96.
56. L. Lin, W. Jiang and P. Xu, *Sci Total Environ*, 2017, **601-602**, 857-864.
57. M. Clara, B. Strenn, O. Gans, E. Martinez, N. Kreuzinger and H. Kroiss, *Water Research*, 2005, **39**, 4797-4807.
58. J. L. Santos, I. Aparicio and E. Alonso, *Environment International*, 2007, **33**, 596-601.
59. B. Kasprzyk-Hordern, R. M. Dinsdale and A. J. Guwy, *Water research*, 2009, **43**, 363-380.
60. A. Joss, S. Zabczynski, A. Göbel, B. Hoffmann, D. Löffler, C. S. McArdell, T. A. Ternes, A. Thomsen and H. Siegrist, *Water research*, 2006, **40**, 1686-1696.
61. C. W. Chow, R. Fabris and M. Drikas, *Journal of Water Supply: Research and Technology-AQUA*, 2004, **53**, 85-92.
62. S. Liu, M. Lim, R. Fabris, C. Chow, K. Chiang, M. Drikas and R. Amal, *Chemosphere*, 2008, **72**, 263-271.
63. Y. Lin, T. V. Williams and J. W. Connell, *The Journal of Physical Chemistry Letters*, 2010, **1**, 277-283.